



Optimal Scheduling for Integrated Hydrogen Production System Based on Exergy Analysis

Mengshu Zhu, Zhiyao Zhong, Jiakun Fang^(✉), and Xiaomeng Ai

Huazhong University of Science and Technology, Wuhan, China
{ms_zhu, zhongzy9803, jfa, xiaomengai}@hust.edu.cn

Abstract. A stable and consistent hydrogen supply is essential in various engineering scenarios. To address the challenge of meeting the demand for stable and green hydrogen with high proportion and fluctuating renewable energy input, integrated hydrogen production systems (IHPS) have been developed. Exergy balance is employed to assess the quality of energy loss and identify the size, location, and influencing factors of energy quality loss, which differs from the traditional scheduling problem of cost minimization or the black box model of exergy analysis. Firstly, the energy conservation principle along with the exergy concept for second-law assessment are applied to each system component. Secondly, an optimal scheduling model for IHPS is established that considers mass, energy, and exergy balance as well as operational constraints. The Pareto front of a multi-objective optimization problem is then established to obtain an optimal scheduling scheme with comprehensive performance in exergy efficiency and economics. Finally, case studies are conducted to intuitively show the distribution of exergy destruction and validate the applicability of the proposed dispatch method in efficiently bringing up a scheduling scheme with better overall performance.

Keywords: Integrated hydrogen production system · Exergy analysis · Exergy loss · Multi-objective optimization

1 Introduction

In recent years, hydrogen has been increasingly recognized as a clean and versatile energy carrier that can contribute to the transition toward a low-carbon economy. Meeting the demand for stable and green hydrogen is critical for many engineering scenarios, including industrial processes, backup power, and hydrogen refueling stations [1]. Fossil fuels are the main source of hydrogen production, causing large pollution. With the increasing use of fluctuating renewable energy for hydrogen production, ensuring a stable hydrogen supply has become a challenge. To address this challenge, integrated hydrogen production systems (IHPS) have been developed as promising solutions that can provide stable and green hydrogen.

The optimal scheduling of different energy sources in IHPS to improve energy efficiency and reduce operating costs remains an active research area. In [2], a basic framework of an integrated energy system containing multiple energy hubs is proposed, and

a distributed economic dispatching model considering carbon emissions is constructed. A deep deterministic policy gradient-based optimal scheduling method for integrated hydrogen energy systems is proposed to minimize the operating cost [3]. Moreover, The exergy, taking into account the “quantity” and “quality” of energy, has attracted the attention of some scholars. Exergy efficiency is used as an objective function to study integrated energy system planning [4]. The influence of the parameters in the integrated system is investigated on exergy and economic indicators through the parametric study to understand the system performance [5]. In summary, traditional scheduling methods often focus on cost minimization or use black box models for exergy analysis, which may not fully capture the quality of energy loss and its influencing factors [6].

This paper proposes an optimal scheduling model for IHPS based on exergy analysis. The scheduling model considers mass, energy, and exergy balance, along with other operation constraints, to obtain a scheduling scheme with comprehensive performance in exergy efficiency and economics. The rest of the paper is organized as follows: Sect. 2 provides an introduction to IHPS and thermodynamic analysis. Section 3 describes the multi-objective optimization scheduling model of IHPS. Section 4 presents the case studies. Section 5 concludes the paper and outlines potential future work.

2 Problem Description and Thermodynamic Analysis

2.1 Problem Description

The primary reason for integrating multiple hydrogen production technologies is that a single hydrogen production process cannot meet the stable and green hydrogen demand. Hydrogen production from fossil fuels leads to high carbon emissions and is not sustainable. On the other hand, renewable energy sources, such as water, biomass, and photovoltaic (wind power), have emerged as sustainable options for hydrogen production. However, hydrogen production from these sources faces challenges, such as fluctuating energy input and material quality issues. For instance, water electrolysis, a promising method for hydrogen production from renewable sources, requires significant energy storage capacity to maintain stable hydrogen output, resulting in high investment costs. Similarly, biomass-based hydrogen production is limited by the availability of biomass, which cannot meet the hydrogen demand.

Therefore, the IHPS has been developed to address these challenges. Figure 1 shows an IHPS combining water electrolysis (WE), biomass gasification (BG), and natural gas reforming (NGR). Energy and materials in the IHPS are coupled and complementarily utilized to increase exergy efficiency and reduce operating costs. Solar power is used by the WE to produce hydrogen and oxygen, with the oxygen either being stored or fed into BG and NGR. The by-product CH_4 from the BG unit can be supplied to NGR. The heat from the BG's outlet gas is used to heat the oxygen through a heat exchanger (HE).

After heating, the feed water at $75.0\text{ }^\circ\text{C}$ and 101.3 kPa enters the WE, which is directly coupled with renewable energy. The water-splitting reaction in the stack generates H_2 in the cathode and O_2 in the anode. The produced O_2 is compressed to 80.0 bar through compression and cooling and stored in a high-pressure tank. For the BG process, the O_2 supplied from the storage tank is depressurized by a direct expansion. The biomass mixed with O_2 is supplied to a gasifier. The heat of the outlet gas is used to improve the

O₂ temperature. After expansion, the stream enters the pressure swing adsorption (PSA) to yield purified H₂ and off-gas (CO₂, CO, and CH₄), which are then fed into the NGR reactor. Additionally, external input gas is also available.

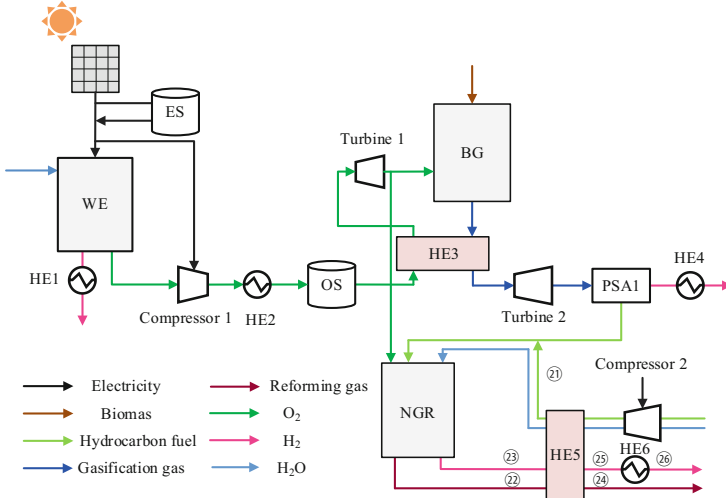


Fig. 1. Flow diagram of the IHPS.

2.2 Modeling and Thermodynamic Analysis

For a general steady-state process, mass and energy balances can be written as:

$$\sum \dot{m}^{in} = \sum \dot{m}^{out} \quad (1)$$

$$\dot{Q} + \sum \dot{m}^{in} h^{in} = \dot{P} + \sum \dot{m}^{out} h^{out} \quad (2)$$

where \dot{Q} is the heat rate, \dot{m}^{in} and \dot{m}^{out} indicate the mass flow rate of inlet and outlet material, \dot{P} is the power, h^{in} and h^{out} are the enthalpy of inlet and outlet material.

Neglecting the potential and kinetic effects, the exergy rate of a fluid stream is shown in (3). The factors $\dot{E}x^{ph}$ and $\dot{E}x^{ch}$ represent the physical and chemical exergy, defined as (4, 5) [7]:

$$\dot{E}x = \dot{E}x^{ph} + \dot{E}x^{ch} \quad (3)$$

$$\dot{E}x^{ph} = \sum_i \dot{m}_i (h_i - h_0 - T_0 (s_i - s_0)) \quad (4)$$

$$\dot{E}x^{ch} = \dot{m} [\sum_i x_i e_{0,i} + RT_0 \sum_i x_i \ln x_i] \quad (5)$$

where T_0 is the standard conditions temperature, R is the ideal gas constant, x_i denotes the mole fraction of i th specie, and e_0 denotes the standard chemical exergy.

The detailed mass, energy, and exergy balance principles of IHPS components are shown in Table 1. The same type of device is not repeatedly enumerated. $\dot{E}x_D$ is exergy destruction of a component in IHPS.

Table 1. Mass, energy, and exergy balance equations for components in the IHPS.

Component	Mass balance	Energy balance	Exergy balance
WE	–	–	$\dot{m}_t^1 ex^1 + \dot{P}_t^{WE} = \dot{m}_t^2 ex^2 + \dot{m}_t^4 ex^4 + \dot{E}x_D^{WE}$
Intercooler1	$\dot{m}_t^2 = \dot{m}_t^3$	$\dot{m}_t^2 h^2 = \dot{m}_t^3 h^3 + H_t^{I1}$	$\dot{m}_t^2 ex^2 = \dot{m}_t^3 ex^3 + \dot{H}_t^{I1} (1 - \frac{T_0}{T_3}) + \dot{E}x_D^{I1}$
Compressor 1	$\dot{m}_t^4 = \dot{m}_t^5$	$\dot{m}_t^4 h^4 + \dot{P}_t^{C1} = \dot{m}_t^5 h^5$	$\dot{m}_t^4 ex^4 + \dot{P}_t^{C1} = \dot{m}_t^5 ex^5 + \dot{E}x_D^{Comp1}$
Turbine1	$\dot{m}_t^8 = \dot{m}_t^9$	$\dot{m}_t^8 h^8 = \dot{m}_t^9 h^9 + \dot{P}_t^{T1}$	$\dot{m}_t^8 ex^8 = \dot{m}_t^9 ex^9 + \dot{P}_t^{T1} + \dot{E}x_D^{T1}$
BG	–	–	$\dot{m}_t^9 ex^9 + \dot{m}_t^{11} ex^{11} = \dot{m}_t^{12} ex^{15} + \dot{E}x_D^{BG}$
HE 1	$\dot{m}_t^7 = \dot{m}_t^8$ $\dot{m}_t^{12} = \dot{m}_t^{13}$	$\dot{m}_t^7 h^7 + \dot{m}_t^{12} h^{12} = \dot{m}_t^8 h^8 + \dot{m}_t^{13} h^{13}$	$\dot{m}_t^7 ex^7 + \dot{m}_t^{12} ex^{12} = \dot{m}_t^8 ex^8 + \dot{m}_t^{13} ex^{13} + \dot{E}x_D^{HE1}$
PSA	$\dot{m}_t^{14} = \dot{m}_t^{15} + \dot{m}_t^{16}$	$\dot{m}_t^{14} h^{14} = \dot{m}_t^{15} h^{15} + \dot{m}_t^{20} h^{20}$	$\dot{m}_t^{14} ex^{14} = \dot{m}_t^{15} ex^{15} + \dot{m}_t^{16} ex^{16} + \dot{E}x_D^{PSA}$
NGR	–	–	$\dot{m}_t^{10} ex^{10} + \dot{m}_t^{18} ex^{21} + \dot{m}_t^{21-H_2O} ex^{21-H_2O} = \dot{m}_t^{22} ex^{22} + \dot{m}_t^{23} ex^{23} + \dot{E}x_D^{FR}$

PEM Electrolyzer. Proton exchange membrane (PEM) has a fast dynamic response and is used as a technology for hydrogen production from water electrolysis. More details and discussions about PEM electrolyzer modeling can be found in [8].

$$\dot{P}_t^{PV} - \dot{P}_t^{PV-cur} - \dot{P}_t^{PV-ES} + \dot{P}_t^{ES-WE} - \dot{P}_t^{C1} - \dot{P}_t^{C2} = \dot{P}_t^{WE} \quad (6)$$

$$\dot{P}_t^{WE} = k_1 N^{cell} U_t^{cell} I_t^{cell} \quad (7)$$

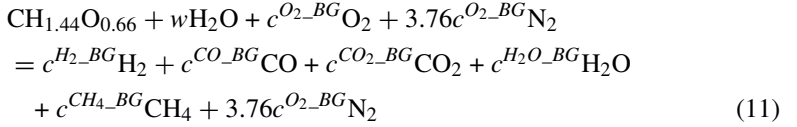
$$U_t^{cell} = E + U_t^{ohm} + U_t^{act} \quad (8)$$

$$I_t^{cell} = A^{cell} i_t^{cell} \quad (9)$$

$$\dot{m}_t^2 = \frac{k_2 N^{cell} I_t^{cell} h^F}{2F}, \dot{m}_t^4 = \frac{k_2 N^{cell} I_t^{cell} h^F}{4F} \quad (10)$$

where \dot{P}^{PV} is the photovoltaic generation, \dot{P}^{PV-cur} is the solar curtailment, \dot{P}_t^{PV-ES} is the power stored to the storage device, \dot{P}_t^{ES-WE} is the energy released from the storage device, \dot{P}_t^{C1} and \dot{P}_t^{C2} denote the power consumed by Compressor 1 and 2, respectively. I^{cell} is WE operating current, N^{cell} is the number of electrolysis cells, U^{cell} is the operating voltage, E is the open circuit voltage, U^{ohm} is the ohmic overvoltage and U^{act} is the activation overvoltage, k_1 and k_2 are unit conversion factor, h^F is Faraday efficiency, F is Faraday constant.

Biomass Gasification Model. The equilibrium model simulates the BG process because it is a reliable way to estimate the composition of syngas [9]. The global gasification reaction using wood as raw material and oxygen as gasifying agent is shown in (11).



where w is the moisture content per mole of wood, c^{O_2-BG} is the oxygen consumption per mole of wood, c^{H_2-BG} , c^{CO-BG} , c^{CO_2-BG} , c^{H_2O-BG} , c^{CH_4-BG} are the output coefficients of H_2 , CO , CO_2 , H_2O , and CH_4 , respectively.

The relationship between biomass feed, oxygen consumption, and gas production can be expressed as (12–14).

$$\dot{m}_t^{12-H_2} = c^{H_2-BG-O_2}\dot{m}_t^{11-O_2} + c^{H_2-BG-Air}\dot{m}_t^{11-Air} \quad (12)$$

$$\dot{m}_t^{9-O_2} = c^{O_2-BG}\dot{m}_t^{11} \quad (13)$$

$$\dot{m}_t^{12-CH_4} = c^{CH_4-BG}\dot{m}_t^{11}, \dot{m}_t^{12-CO_2} = c^{CO_2-BG}\dot{m}_t^{11} \quad (14)$$

Natural Gas Reforming Model. Chemical-looping auto-thermal reforming (CLRa) is applied to smooth out the fluctuations, which can achieve CO_2 capture without additional hydrogen purification. The detailed reactions and processes can be found in [10]. The product compositions are calculated by the reaction equilibrium based on gibbs minimization, mass balance, and heat balance equations. The products can be calculated in (15, 16). The temperature of the inlet gas will affect the coefficient in (17).

$$\dot{m}_t^{23} = c_t^{H_2-NGR-O_2}\dot{m}_t^{18-CH_4-O_2} + c_t^{H_2-NGR-Air}\dot{m}_t^{18-CH_4-Air} \quad (15)$$

$$\begin{aligned} \dot{m}_t^{10} &= c_t^{O_2-NGR}\dot{m}_t^{18-CH_4-O_2}, \dot{m}_t^{22-H_2O} \\ &= c_t^{H_2O-NGR}\dot{m}_t^{21-CH_4} \end{aligned} \quad (16)$$

$$c_t^Y = f(T_t^{NGR}), Y \in \{\text{H}_2, \text{O}_2, \text{H}_2\text{O}, \text{CO}_2\} \quad (17)$$

3 Multi-objective Scheduling Optimization Model for IHPS

3.1 Objective Function

The objective function includes exergy efficiency and economy, where exergy efficiency is considered from the perspective of energy loss.

Exergy loss model of the exergy efficiency objective function. Energy efficiency utilization evaluates the utilization of energy in terms of quantity. However, the behavior of converting high-quality energy (e.g., electrical energy) to low-quality energy (e.g., thermal energy) may occur. Exergy efficiency evaluates how well energy is utilized to achieve high-quality utilization of different energy sources, such as energy cascade use. The exergy loss is regarded as the objective function to cut the wastage of high-quality energy in (18). The exergy loss of the IHPS is determined by adding up the exergy destruction of each component.

$$F^{ExD} = \dot{E}x_D^{WE} + \dot{E}x_D^{BG} + \dot{E}x_D^{NGR} + \dot{E}x_D^{I1} + \dot{E}x_D^{I2} + \dot{E}x_D^{I3} + \dot{E}x_D^{I4} + \dot{E}x_D^{HE1} + \dot{E}x_D^{HE2} + \dot{E}x_D^{Comp1} + \dot{E}x_D^{Comp2} + \dot{E}x_D^{Turb1} + \dot{E}x_D^{Turb2} + \dot{E}x_D^{PSA} \quad (18)$$

Mathematical model of the economic objective function. The main component of the economic objective function is the operating cost. It consists of biomass and gas purchase costs.

$$F^{Eco} = \sum_t \left(\mu_{raw}^{bio} m_t^{11} + \mu_{raw}^{gas} m_t^{19} \right) \quad (19)$$

where μ_{raw}^{bio} and μ_{raw}^{gas} is the price per unit of biomass and natural gas.

3.2 Operation Constraints

Stable Hydrogen Production Constraints. The sum of hydrogen production of each module should meet the stable demand N^{H2} .

$$k_2 * \Delta t * (m_t^3 + m_t^{17} + m_t^{23}) = N^{H2} \quad (20)$$

Operation Constraints of Hydrogen Production Unit.

$$0 \leq P_t^{WE} \leq P^{WE_max}, 0 \leq m_t^{11} \leq m^{11_max}, 0 \leq m_t^{18} \leq m^{18_max} \quad (21)$$

where P^{WE_max} is the maximum output of WE unit, m^{11_max} and m^{18_max} are the maximum input of biomass and gas.

Energy Storage Device Operation Constraints.

$$\begin{aligned} Q_t^{ES} &= Q_{t-1}^{ES} + \eta^{ES} P_t^{PV_ES} - P_t^{ES_WE} / \eta^{ES} \\ 0 &\leq Q_t^{ES} \leq Q^{ES_max}, Q_1^{ES} = Q_T^{ES}, \\ 0 &\leq P_t^{PV_ES} \leq s_t^{ES} P^{ES_max}, 0 \leq P_t^{ES_WE} \leq (1 - s_t^{ES}) P^{ES_max} \end{aligned} \quad (22)$$

where Q^{ES} is the capacity of energy storage, Q^{ES_max} and P^{ES_max} are the upper limit of the capacity and storage/release power of storage, s^{ES} is the 0–1 state variable.

Oxygen and electricity storage constraints are similar and will not be reiterated.

3.3 Multi-objective Processing

For convex optimization problems, when the weight vector λ composed of multiple objective weights is non-negative, the scaling method can obtain the optimal solution on all Pareto front. The original objective (24) can be transferred to (25). Standardizing and normalizing the objective function allows for screening solutions that meet IHPS's multi-objective optimization scheduling requirements from the Pareto front.

$$\min f = (F^{ExD}, F^{Eco}) \quad (23)$$

$$\min \lambda^T f = \lambda^{ExD} F^{ExD} + \lambda^{Eco} F^{Eco} \quad (24)$$

4 Case Studies

Table 2 introduces the input values for the parameters in the study. The proposed problem is implemented to obtain the 24-h scheduling results.

4.1 Multi-objective Optimal Scheduling Results and Comparative Analysis

Multi-objective optimization problems are quantified, and enough Pareto optimal solutions are found by traversing the weight method. The specified weight's traversal step size is 0.01, which is solved by MATLAB R2022b and Gurobi 9.5.2. The Pareto frontier is obtained by interpolation fitting of the Pareto optimal solution in Fig. 2.

Table 3 presents a comparison of scheduling results obtained using different dominant objective functions. At the maximum operating cost, there is a 12.85 MW difference between the exergy loss and the minimum value, accounting for 32% of the total. The operating cost under the minimum destruction differs from the minimum cost by 839.51 \$, accounting for 21%. Under the cost-dominant scheme, the WE output contributes significantly because the cost of renewable energy is not considered. On the other hand, the NGR output increases significantly in a loss-dominated scheme due to its higher exergy efficiency compared to other technologies. The proposed method effectively balances the economic and efficiency aspects.

4.2 Exergy Analysis of IHPS

Figure 3 illustrates the exergy distribution of IHPS under the multi-objective optimal scheduling results. Although the input biomass exhibits high exergy, the exergy of output hydrogen is the lowest among the three technologies indicating that the exergy efficiency of BG is relatively low. In contrast, NGR has the lowest exergy input and the highest exergy of hydrogen, with the highest exergy efficiency. The analysis reveals that the WE

Table 2. Input data for major parameters for modeling the system.

Paraments	Value
Stable hydrogen demand, N^{H_2}	1000 Nm ³ /h
Maximum power of WE units, P^{WE_max}	5 MW
Maximum feed rates of BG/NGR units, m^{11_max}/m^{18_max}	0.36/0.05 kg/s
Energy and oxygen storage capacity, Q^{ES_max}	4 MW
Upper limit rate of storage/release oxygen/power, P^{ES_max}	2 MW
Average air temperature surrounding the system, T_0	293.15 K
Average air pressure surrounding the system, P_0	101.3 kPa
Temperature/pressure of WE unit	350 K, 101.3 kPa
Temperature/pressure of BG unit	1100 K, 24 bar
Temperature/pressure of NGR unit	1100 K, 12 bar
Faraday constant, F	96458 C/mol
Gas constant, R	8.314 J/mol·K
Number of cells in the stack, N^{cell}	350
Active service area, A^{cell}	1200 cm ²
Faraday efficiency, h^F	0.99
Moisture content per mol of wood, w	10%

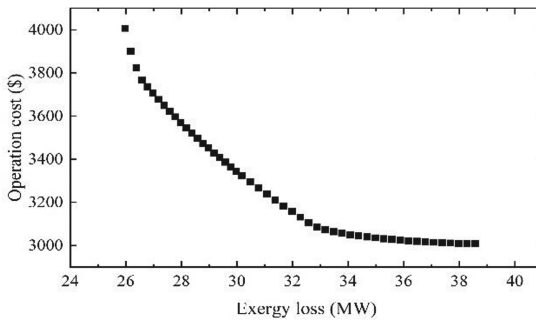


Fig. 2. Pareto front for IHPS multi-objective optimal scheduling.

module experiences the highest exergy destruction due to its numerous components and physical transformation processes, including compression and cooling, which can cause partial exergy destruction.

Figure 4 illustrates the various subcomponents and their associated exergy destruction rates under an optimal scheduling scheme. The main destructions exist in WE, BG, and NGR, where chemical reactions occur. Even though the hydrogen production from NGR is the largest in this scenario, the destruction is less than that from WE and BG.

Table 3. Scheduling results dominated by different objective functions.

Objective function	Minimum operating cost	Minimum exergy loss	Multi-objective optimization
Operating cost (\$)	3010.16	4007.54	3049.59
Exergy loss (MW)	38.70	26.01	33.37
Hydrogen from WE (Nm ³)	8660.52 (36%)	4016.20 (16%)	8163.47 (34%)
Hydrogen from BG (Nm ³)	13,198.67 (55%)	4202.27 (18%)	6858.48 (29%)
Hydrogen from NGR (Nm ³)	2140.82 (9%)	1,5781.53 (66%)	8978.05 (37%)

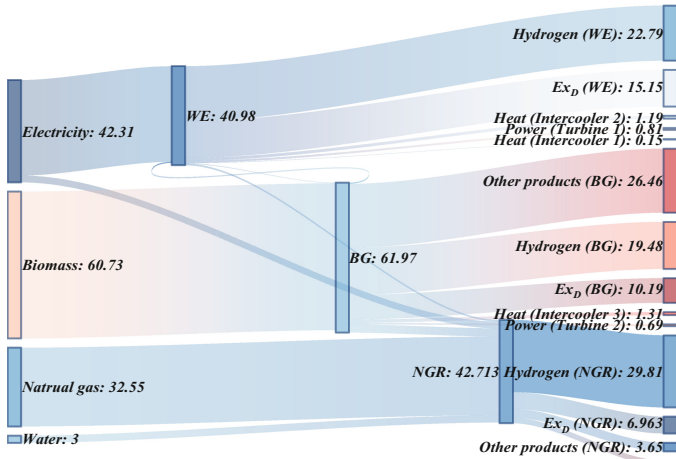


Fig. 3. Sankey diagram of exergy distribution in IHPS (unit: MW).

The exergy destruction from WE is larger than that from BG due to its more considerable input and mass flow rate.

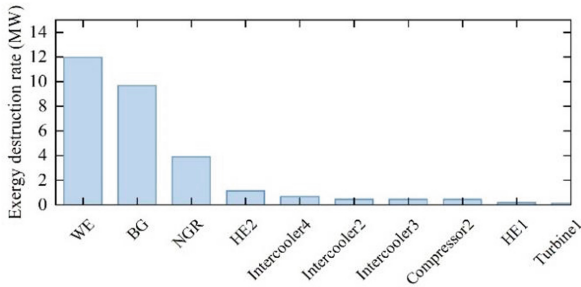


Fig. 4. Main components with respective exergy destruction rates.

5 Conclusion

This paper proposes an optimal scheduling model for IHPS based on exergy analysis. The proposed scheduling model considers mass, energy, and exergy balance, as well as other operational constraints, to develop a scheduling scheme that optimizes both exergy efficiency and economics. Case studies demonstrate the Pareto front and the scheduling results for balancing exergy efficiency and operating costs based on specific needs and goals. Moreover, the exergy distribution and exergy destruction are developed to quantify energy quality and loss in IHPS, which can assist energy managers in identifying areas where energy is being wasted and provide insights on how to improve the overall efficiency of IHPS.

Acknowledgment. The paper is funded by the National Natural Science Foundation of China, Grant ID: 52177088, and the National Natural Science Foundation of China, Grant ID: 52177089.

References

1. Song, P., Sui, Y., Shan, T., et al.: Assessment of hydrogen supply solutions for hydrogen fueling station: a Shanghai case study. *Int. J. Hydrogen Energy* **45**(58), 32884–32898 (2020)
2. Ma, L., Liu, N., Zhang, J., et al.: Real-Time rolling horizon energy management for the energy-hub-coordinated horizon energy management for the energy-hub-coordinated prosumer community from a cooperative perspective. *IEEE Trans. Power Syst.* **34**(2), 1227–1242 (2019)
3. Li, H., Qin, B., Jiang, Y., et al.: Data-driven optimal scheduling for underground space based integrated hydrogen energy system. *IET Renew. Power Gener.* **16**(12), 2521–2531 (2022)
4. Hu, X., Zhang, H., Chen, D., et al.: Multi-objective planning for integrated energy systems considering both exergy efficiency and economy. *Energy* **197**, 117155 (2020)
5. Habibollahzade, A., Gholamian, E., Ahmadi, P.: Multi-criteria optimization of an integrated energy system with thermoelectric generator, parabolic trough solar collector and electrolysis for hydrogen production. *Int. J. Hydrogen Energy* **43**(31), 14140–14157 (2018)
6. Li, J., Wang, D., Jia, H., et al.: Mechanism analysis and unified calculation model of exergy flow distribution in regional integrated energy system. *Appl. Energy* **324**, 119725 (2022)
7. Montazerinejad, H., Fakhimi, E., Ghandehariun, S., et al.: Advanced exergy analysis of a PEM fuel cell with hydrogen energy storage integrated with organic Rankine cycle for electricity generation. *Sustain. Energy Technol. Assess.* **51**, 101885 (2022)

8. Xing, X., Lin, J., Song, Y., Song, J., Mu, S.: Intermodule management within a large-capacity high-temperature power-to-hydrogen plant. *IEEE Trans. Energy Convers.* **35**(3), 1432–1442 (2020)
9. Cao, Y., Dhahad, H.A., Togun, H., et al.: A novel hybrid biomass-solar driven triple combined power cycle integrated with hydrogen production: multi-objective optimization based on power cost and CO₂ emission. *Energy Convers. Manage.* **234**, 113910 (2021)
10. Kang, K., Kim, C., Bae, K., et al.: Oxygen-carrier selection and thermal analysis of the chemical-looping process for hydrogen production. *Int. J. Hydrogen Energy* **35**(22), 12246–12254 (2010)